Detecting opaque and nonopaque tropical upper tropospheric ice clouds: A trispectral technique based on the MODIS 8–12 μm window bands

Gang Hong,[1] Ping Yang,[1] Andrew K. Heidinger,[2] Michael J. Pavolonis,[2] Bryan A. Baum,[3] and Steven E. Platnick[4]

[1] A trispectral technique is developed for detecting tropical upper tropospheric opaque ($\tau > 6$) and nonopaque ($\tau < 6$) ice clouds over ocean based on the brightness temperature differences between the MODIS 8.5 and 11 μm bands and between the 11 and 12 μm bands together with the MODIS detected cloud thermodynamic phase. The brightness temperature differences provide robust information for classifying ice clouds, as illustrated by the observations made by a lidar, a radar, and the MODIS Airborne Simulator over tropical ice anvil systems during the Cirrus Regional Study of Tropical Anvils and Cirrus Layers-Florida Area Cirrus Experiment. The trispectral technique for detecting tropical upper tropospheric opaque and nonopaque ice clouds is developed based on the analysis of 1 year of data, including MODIS infrared brightness temperatures at 8.5, 11, and 12 μm bands, MODIS-derived ice cloud optical thicknesses, and cloud top heights from CALIPSO and CloudSat over a region (140°E–180°E, 0°N–20°N) in the Western Pacific Warm Pool. The accuracy of the present trispectral technique is above 80%. A 27 July 2007 MODIS granule over the chosen region is used to verify the trispectral technique. It is found that the classification from the trispectral technique is consistent with a classification based directly on the MODIS ice cloud optical thicknesses. The effects of the variations in the MODIS viewing zenith angle on the detection are found to be negligible. The CALIPSO and CloudSat observations used to develop the classification are more sensitive than MODIS to the height and presence of optically thin cirrus. These differences in cloud heights were found to have a negligible impact on the final detection results.

Citation: Hong, G., P. Yang, A. K. Heidinger, M. J. Pavolonis, B. A. Baum, and S. E. Platnick (2010), Detecting opaque and nonopaque tropical upper tropospheric ice clouds: A trispectral technique based on the MODIS 8–12 μm window bands, *J. Geophys. Res.*, *115*, D20214, doi:10.1029/2010JD014004.

1. Introduction

[2] Ice clouds occur in up to 70% of the tropical tropopause region [*Wang et al.*, 1996] and have a significant impact on the radiation balance, water content and chemical balance of the stratosphere and, as a result, on the tropospheric climate [*Ramanathan and Collins*, 1991; *McFarquhar et al.*, 2000; *Gao et al.*, 2004; *Stephens*, 2005; *Tian et al.*, 2005; *Comstock et al.*, 2007; *Gettelman and Birner*, 2007; *Eguchi et al.*, 2007; *Fu et al.*, 2007]. Ice clouds in the upper troposphere have been

suggested as providing a mechanism for the dehydration of air associated with troposphere-to-stratosphere transport [*Gettelman et al.*, 2002; *Luo et al.*, 2003; *Jensen and Pfister*, 2004; *Dessler et al.*, 2006; *Immler et al.*, 2007]. An understanding of the formation, maintenance and dissipation of upper tropospheric tropical ice clouds is important for investigating the mechanisms of the tropical tropopause layer dehydration [*Gettelman et al.*, 2002; *Luo et al.*, 2003; *Jensen and Pfister*, 2004; *Hong et al.*, 2005; *Dessler et al.*, 2006; *Immler et al.*, 2007].

[3] As discussed in previous studies [e.g., *Ramanathan and Collins*, 1991], ice clouds have two competing effects on the Earth's radiation budget. The ice clouds can reduce the solar radiation reaching the Earth by reflecting a portion of the incoming solar radiation back into space. Ice clouds reduce the outgoing longwave radiation (OLR) and warm the atmosphere through the absorption of a portion of the upwelling IR radiation emitted by the lower atmosphere and the Earth's surface and by the emission of IR radiation at lower temperatures. The net radiative effect of tropical ice

[1]Department of Atmospheric Sciences, Texas A&M University, College Station, Texas, USA.
[2]NOAA/NESDIS Center for Satellite Applications and Research, Madison, Wisconsin, USA.
[3]Space Science and Engineering Center, University of Wisconsin Madison, Madison, Wisconsin, USA.
[4]Laboratory for Atmospheres, NASA-GSFC, Greenbelt, Maryland, USA.

clouds depends on the micro/macrophysical and optical properties of the clouds [*Poetzsch-Heffter et al.*, 1995; *Hartmann et al.*, 2001; *Stephens*, 2005; *Hong et al.*, 2007a]. The radiative impact has been proposed as a possible mechanism affecting the rate of air mass transport from the troposphere to the stratosphere [*Corti et al.*, 2006; *Huang and Su*, 2008].

[4] Various cloud types affecting the Earth's radiation budget have been investigated by different methods [*Poetzsch-Heffter et al.*, 1995; *Rossow and Zhang*, 1995; *Zhang et al.*, 1995; *Chen et al.*, 2000; *Hartmann et al.*, 2001]. Nonopaque ice clouds, defined as transmissive ice clouds (clouds with a visible optical thickness less than 5–6), and opaque ice clouds, defined as nontransmissive ice clouds (clouds with a visible optical thickness of about 5–6 or greater) [*Pavolonis et al.*, 2005; *Wylie et al.*, 2005; *Stubenrauch et al.*, 2006], can have opposing effects on the radiation forcing at the top of atmosphere (TOA). *Poetzsch-Heffter et al.* [1995] found that high-transmittance ice clouds (visible optical thickness less than 3.6) have a warming effect with a value of about 2 W m^{-2} on the radiative forcing at the top of atmosphere, while low-transmittance ice clouds (visible optical thickness greater than 9.4) have a cooling effect with an approximate value of -4 W m^{-2}. To better understand the radiative effect of ice clouds, part of our motivation for this study is to classify ice clouds as being either nonopaque or opaque [*Poetzsch-Heffter et al.*, 1995; *Chen et al.*, 2000].

[5] Three algorithms for determining cloud type, including opaque and nonopaque ice clouds, from visible, near-infrared, and infrared satellite imaging data are described by *Pavolonis et al.* [2005]. Two of the three algorithms, based on 0.65, 1.6, 3.75, 10.8, and 12.0 μm spectral band data from the advanced very high resolution radiometer (AVHRR) on board National Oceanic and Atmospheric Administration (NOAA) satellites, are used operationally in NOAA's extended clouds from AVHRR (CLAVR)-x processing system. The third algorithm uses spectral bands of 0.65, 1.38, 3.75, 8.5, 10.8, and 12 μm available from the moderate resolution imaging spectroradiometer (MODIS). All these spectral bands will be available on the visible-infrared imaging radiometer suite (VIIRS) on board the National Polar-Orbiting Operational Environmental Satellite System (NPOESS), the next generation of low Earth orbiting environmental satellites and the first NPOESS satellite was scheduled to launch in 2010s. The above approaches rely on solar illumination as they use visible and near-infrared measurements.

[6] The detection of clouds using IR measurements has a distinct advantage over the visible/near-infrared techniques by providing consistent data regardless of solar illumination. Bispectral split-window techniques have been suggested [*Inoue*, 1987, 1989] and developed to the point where it has been applied to decades of AVHRR data [*Heidinger and Pavolonis*, 2009]. A bispectral technique based on data at 8.5 and 11 μm is used to derive the cloud thermodynamic phase [*Baum et al.*, 2003], and trispectral techniques have been developed to infer cloud thermodynamic phase based on the variations of the brightness temperature differences (BTD) at 8.5 and 11.0 μm [BTD(8.5–11)] and between 11.0 and 12.0 μm [BTD(11–12)] [*Ackerman et al.*, 1990; *Strabala et al.*, 1994; *Menzel et al.*, 2008]. Until the early

1990s, no single operational satellite imager provided the three bands of 8, 11, and 12 μm, and the trispectral techniques to determine cloud thermodynamic phase combined measurements from different sensors [*Ackerman et al.*, 1990; *Strabala et al.*, 1994].

[7] *Ackerman et al.* [1990] established the trispectral technique on the basis of these brightness temperature differences for detecting cirrus clouds using measurements from the high spectral resolution interferometer sounder (HIS) and cloud and aerosol lidar (CALS) taken on board the ER-2 on 28 October 1986. Their method identifies cirrus clouds by positive brightness temperature differences between both 8 and 11 μm and 11 and 12 μm. The trispectral technique was further investigated by *Strabala et al.* [1994] for detecting cloud and cloud properties. Using mainly observations at the three bands from MODIS airborne simulator (MAS) from 5 December 1991 ER-2 flight, the thresholds to identify ice cloud with emissivity near one and ice cloud with emissivity less than one are developed. They also developed thresholds for clear sky over water, water, and mixed phase clouds. Both of the trispectral techniques by *Ackerman et al.* [1990] and *Strabala et al.* [1994] are pioneer studies on detecting clouds using infrared measurements from satellites, particularly MODIS sensor that was launched on the Terra platform in December 1999 and was the first satellite imager to provide measurements in all three spectral bands of 8.5, 11, and 12 μm.

[8] In addition to these three spectral bands, *Lutz et al.* [2003] used bands at 3.9 and 6.2 μm to determine properties for relatively thin cirrus and other cloud types. The bands of 3.75, 11.0, and 12.0 μm were used for nighttime retrievals of cloud temperature, particle size, and optical thickness [*Minnis et al.*, 1995, 1998]. *Kahn et al.* [2005] presented a thin cirrus detection technique based on the 3.8 and 10.4 μm brightness temperature difference. Cloud effective emissivity ($N\varepsilon$) has been derived from the high-resolution infrared radiometer sounder (HIRS) [*Wylie and Menzel*, 1999; *Wylie et al.*, 2005; *Stubenrauch et al.*, 2006]. A $N\varepsilon$ of 0.95 corresponds approximately to a visible optical thickness of 6 and can be used to classify upper tropospheric ice clouds into opaque and nonopaque ice clouds.

[9] The goal of this research is to discriminate between opaque and nonopaque ice clouds based on the trispectral technique, which is particularly important for ice cloud detection when there is little or no solar illumination. Since the MODIS aboard Terra was launched in December 1999, several instruments measuring the spectral bands of 8–12 μm have been placed on other satellites successfully launched into space. The instruments are the MODIS and atmospheric infrared sounder (AIRS) aboard the Aqua satellite launched in May 2002; the spinning enhanced visible and infrared imager (SEVIRI) aboard the Meteosat Second Generation (MSG) satellite launched in August 2002; the tropospheric emission spectrometer (TES) aboard the Aura satellite launched in July 2004; and the infrared atmospheric sounding interferometer (IASI) aboard the MetOp satellite launched in October 2006. With the large number of satellite measurements now available, it would be interesting to explore the possibility for classifying opaque and nonopaque ice clouds that are consistent with those identified

Table 1. Spectral and Radiometric Characteristics of MAS Spectral Bands During CRYSTAL-FACE Used in This Study

MAS Band	Equivalent MODIS Bands	MAS Mean Wavelength (μm)	Spectral Resolution (μm)	Equivalent Noise[a]	Principal Absorption Components
2	1	0.65	0.053	0.157	H_2O, O_3
20	7	2.15	0.057	0.003	H_2O, CO_2, CH_4, N_2O
42	29	8.52	0.44	0.14	H_2O, O_3, CH_4, N_2O
45	31	11.0	0.54	0.10	H_2O, CO_2
46	32	12.0	0.45	0.19	H_2O, CO_2

[a]Noise equivalent (W m^{-2} μm^{-1} sr^{-1}) for channels 2 and 20; noise equivalent temperature difference (K) for channels 42, 45, and 46.

directly from the visible retrieved ice cloud optical thickness using the IR trispectral technique.

[10] This paper reports on a technique for classifying upper tropospheric ice clouds into opaque and nonopaque categories using MODIS observations made at 8.5, 11, and 12 μm to detect ice clouds in the nighttime. In section 2, the integrated measurements taken from the NASA ER-2 aircraft during the 2002 Cirrus Regional Study of Tropical Anvils and Cirrus Layers-Florida Area Cirrus Experiment (CRYSTAL-FACE), including observations made by a cloud lidar, a radar, and an airborne scanning spectrometer covering visible to IR bands, are used to investigate the features of the variations between BTD(8.5–11) versus BTD (11–12) for ice clouds. In section 3, the MODIS retrieved ice cloud optical thickness, the MODIS measurements of IR brightness temperatures at 8.5, 11, and 12 μm bands, and the CloudSat and CALIPSO cloud products are used to develop a trispectral technique for classifying upper tropospheric opaque and nonopaque ice clouds. Section 4 reports on the classification of a MODIS granule using the present trispectral technique combined with the estimated cloud top heights from MODIS IR measurements, and the effects of cloud top and sensor zenith angle on the results are investigated. Section 5 summaries this study.

2. Trispectral Features at 8.5, 11, and 12 μm From Airborne Measurements

2.1. NASA ER-2 Airborne Data in the CRYSTAL-FACE

[11] CRYSTAL-FACE, performed in July 2002, was a measurement campaign to investigate tropical upper tropospheric cirrus cloud systems (http://www.espo.nasa.gov/crystalface/science.html). The CRYSTAL-FACE experiment was aimed at a better understanding of the microphysical properties and formation processes of the clouds using a combination of measurements and modeling capabilities [Jensen and Pfister, 2004]. Six aircraft and several surface sites were used to collect data in areas near Florida and the Caribbean Sea. The NASA ER-2, carrying both active and passive radiometers, was flown in the lower stratosphere and used primarily for remote sensing. The MODIS airborne simulator (MAS), cloud physics lidar (CPL), and cloud radar system (CRS), aboard the ER-2, have supported development of satellite retrieval schemes by MODIS, Cloud-Aerosol Lidar and Infrared Pathfinder Satellite Observation (CALIPSO), and CloudSat, which are part of the NASA A-Train satellite constellation. In this study, measurements taken from the MAS, CPL, and CRS are used to investigate the spectral characteristics of clouds in the 8.5, 11, and 12 μm bands.

[12] The MAS is a cross-track scanning spectrometer that measures reflected solar and emitted thermal radiation in 50 narrowband channels in the range of 0.55–14.3 μm. With each pixel having a 0.14° instantaneous field of view, the spatial resolution at nadir is 50 m at a nominal aircraft altitude of 20 km. The cross-track scan angle of 85.92° (±42.96°from nadir) corresponds to a ground swath of about 37.25 km at an altitude of 20 km. There are a total of 716 Earth-viewing pixels per sensor scan. See a detailed discussion on MAS in the work of Hook et al. [2001]. With a much higher spatial resolution than the other instruments, MAS provides more information on the small-scale distribution of various atmospheric parameters [King et al., 1996]. Ten spectral bands of MAS were generally used in the cloud mask and the cloud optical property retrievals [King et al., 2004]. The MAS infrared spectral bands were used to study the cloud thermodynamic phase, the cloud top height and the cloud fraction [Baum et al., 2000]. Table 1 lists the spectral and radiometric characteristics of the MAS spectral bands from the CRYSTAL-FACE experiment used in this study.

[13] The CPL is a three-wavelength (0.355, 0.532, and 1.064 μm) backscatter lidar [McGill et al., 2002, 2004]. It scans downward from the ER-2 with a vertical resolution of 30 m and a 1 s temporal resolution (about 200 m at an average ER-2 ground speed of about 200 m s^{-1}). The CRS [Racette et al., 2003; Li et al., 2004] is a 94 GHz pulsed polarimetric Doppler radar. The CRS measurements have a vertical resolution of 37.5 m and temporal resolution of 0.5 s. Detailed descriptions of the CPL and the CRS can be found in McGill et al. [2004]. Since lidar is more sensitive to small ice particles and optically thin cirrus clouds than radar, lidar can profile optically thin cirrus clouds frequently missed by radar and radar can detect optically thick clouds impenetrable by lidar signals. Because of the difference in sensitivity, lidar is mainly used for optically thin ice clouds and radar for optically thick clouds. The complementary nature of the combined CPL and CRS measurements from CRYSTAL-FACE were used for our cloud studies [McGill et al., 2004]. In this study, the CPL-derived cloud top height and the CRS reflectivity are used to define the vertical structures of ice clouds. A convective anvil was generated along the west coast of Florida on 29 July 2002 and, during the early evening, produced an extensive ice cloud deck varying from thin cirrus to thick ice clouds. The measurements taken from three flight tracks over the convective anvil system with the MAS, CPL, and CRS instruments operated simultaneously are chosen for this study. Figure 1 shows the three flight tracks labeled as tracks 14, 15, and 16.
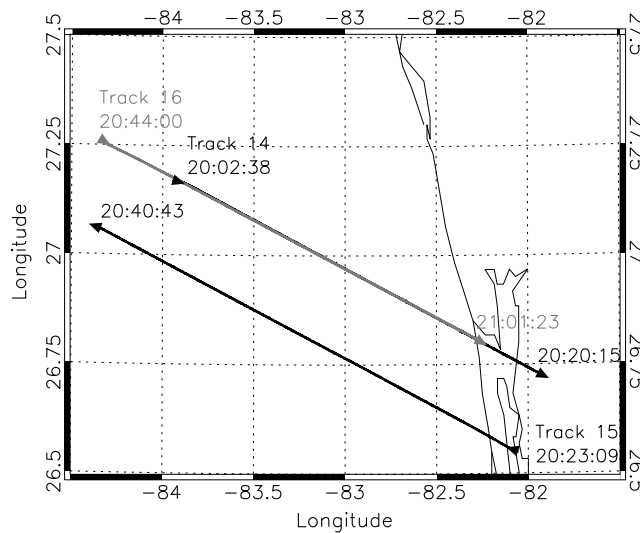
**Figure 1.** ER-2 flight tracks 14–16 for 29 July 2002 used in this study.

2.2. Properties of IR Radiances at 8.5, 11, and 12 μm of MAS

[14] The MAS measurements along flight track 16 made on 29 July 2002 are shown in Figure 2. The swath section is 338 × 37 km covering 6498 scan lines between 20:44:00 and 21:01:23. In the false color phase image (Figure 2a), the MAS band 2 reflectance (0.65 μm) is mapped in red, the band 20 reflectance (2.13 μm) is mapped in green, and the band 45 brightness temperature (11 μm) is mapped in blue, with the scale reversed so that cold clouds have higher contrast. In the false RGB image, the ocean is dark, thin cirrus clouds are light blue, and optically thick ice clouds are purple. The clouds in the scene are mainly thin and thick ice clouds, and thin ice clouds appear to develop around the edges (around 20:50:00) of thick ice clouds.

[15] Large brightness temperature depressions at the MAS 8.5 and 11 μm channels (Figures 2b and 2c) occur over the regions with optically thick ice clouds. BT(11) has distinct brightness temperature depressions over the transitional zone from optically thin to thick clouds. This feature is clearly shown in the image of BTD(8.5–11) (Figure 2d) with large positive values of BTD(8.5–11) (from 20:46:00 to 20:50:00). Negative values of BTD(11–12) are observed mainly over optically thick ice clouds whereas those of BTD (8.5–11) can be over optically thin (20:45:00 to 20:47:00) and thick ice clouds (>20:50:00) or clear sky (<20:45:00). The large positive BTD(11–12) is found to be farther away from the edge of thick ice clouds than the BTD(8.5–11). These features of BTD(8.5–11) or BTD(11–12) have been used to classify clouds solely or with a combination of BT (8.5), BT(11), or BT(12) [e.g., *Inoue*, 1987, 1989; *Ackerman et al.*, 1990; *Strabala et al.*, 1994].

[16] The CRS reflectivity profiles over the ice anvil cloud system along flight track 16 are shown in Figure 3a. The black curve above the radar reflectivity indicates the cloud top estimated from the CPL measurements. Evidently, this anvil system penetrated into the TTL with a cloud top of above 12 km. On the basis of the CPL and CRS measurements, the anvil system is separated into four parts indicated
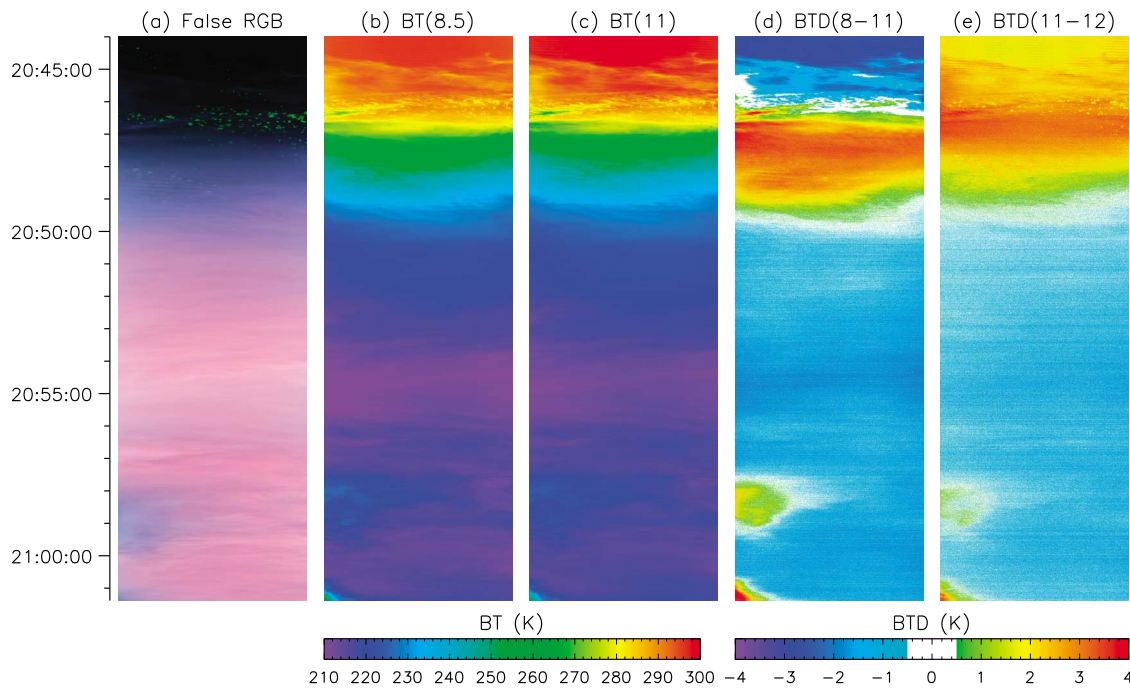
Figure 2. MODIS airborne simulator (MAS) images of the 353 × 37 km section of the flight track 16 shown in Figure 1 on 29 July 2002 (6566 scan lines between 20:44:00 and 21:01:23). (a) The false RGB image based on MAS bands 2, 20, and 45 (gray flipped) (see details in text). (b and c) Brightness temperatures at 8.5 and 11.0 μm, respectively. (d and e) Brightness temperature differences BTD(8.5–11) and BTD(11–12), respectively.
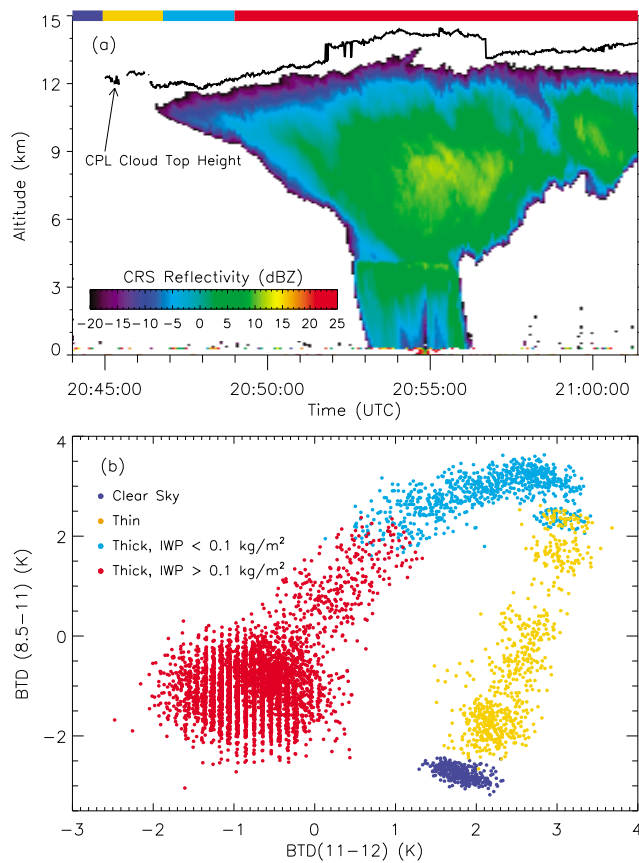
Figure 3. (a) CRS reflectivity profiles over an ice anvil cloud system along the flight track 16. The black curve above the radar reflectivity indicates the cloud top estimated from the CPL measurements. The color bars in the upper x axis indicates different portions of the cloud system, which are used for the diagram of BTD(11–12) and BTD(8.5–11) shown in Figure 3b. In Figure 3a, the gap between CPL derived cloud tops and radar top reflectivity is mainly due to the CRS radar's sensitivity as it only measures clouds down to −26 dBZ.

by the color bars in the upper x axis. The first part, indicated by a blue bar, is over clear sky where neither CRS nor CPL has a signal. The second part, indicated by an orange bar, is over thin cirrus clouds to which CPL is sensitive but CRS is either not sensitive or the CRS reflectivity is less than −20 dBZ. The third part, indicated by a light blue bar, derived from CRS reflectivities, corresponds to thick ice clouds having ice water paths (IWP) less than 100 g m^{-2}. An ice water path (IWP) of 100 g m^{-2} is approximately a visible optical thickness of $\tau = 5.43 - 6.15$ using $\tau = 3Q_e\text{IWP}/D_e\rho_{ice}$ [e.g., *Hong et al.*, 2008], where Q_e is the mean effective efficiency (about 2 for visible bands), D_e is effective particle size (its climatological mean values of 60.0 μm for high clouds from the ISCCP [International Satellite Cloud Climatology Project) measurements [*Rossow and Schiffer*, 1999] and 53 μm for high clouds from 3 years of MODIS measurements [*Hong et al.*, 2007b] correspond to $\tau = 5.43$ and 6.13, respectively], and ρ_{ice} is ice density of 0.917×10^3 kg/m^3. The fourth and final parts, indicated by a red bar, are associated with thick ice clouds with ice water

paths greater than 100 g m^{-2}. The relationships between the BTD(8.5–11) and BTD(11–12) corresponding to the four parts are shown in Figure 3b. Distinct separations are shown for the four types of regions.

[17] The characteristics of trispectral measurements are attributed to the combined effects of atmospheric absorption, ice cloud absorption and scattering. The atmospheric absorption at 8.5 μm is much stronger than those of 11.0 and 12.0 μm [*Hong et al.*, 2007a]. For ice, the bands at 11.0 and 12.0 μm have much larger values of the imaginary index of refraction than the band at 8.5 μm. This divergence in the imaginary part of the refractive index of ice in the three bands has been used as the basis for a method to infer particle thermodynamic phase using the three bands [*Baum et al.*, 2000, and references therein]. Single-scattering albedos ω of various cirrus clouds were investigated by *Baum et al.* [2000] and *Hong et al.* [2007a], and ω at 8.5 μm was found to be larger than at 12.0 μm or at 11.0 μm. For thin cirrus clouds (Figure 3b), when the optical thicknesses are small, atmospheric absorption plays a major role and BTD(8.5–11) is negative. With increasing optical thickness, both ice particle absorption and scattering increase and BTD (8.5–11) become positive. In the thin cirrus cloud region, BTD(11–12) increases to its maximum with the increase of optical thickness since ice particle absorption (playing the main contribution) and scattering at 12.0 μm are stronger than those at 11.0 μm. In thick ice cloud region, with an increase in optical thickness, the scattering effects of ice clouds on the three bands tend to be saturated. BTD(8.5–11) and BTD(11–12) decrease from their maximum positive values. With continuously increasing optical thickness, BTD (8.5–11) and BTD(11–12) accumulate around their asymptotic values since, in terms of the upwelling radiation, the ice cloud behaves like a blackbody at nearly the cloud top temperature. These features from observations are consistent with model simulations [e.g., *Baum et al.*, 2000; *Pavolonis et al.*, 2005; *Nasiri and Kahn*, 2008].

[18] With the use of the same cloud types as in Figure 3, the cloud systems along tracks 14 and 15 are also classified. The features of BTD(8.5–11) and BTD(11–12) for each specific cloud type along the two tracks are consistent with those along the track 16. It is evident that variations of BTD (8.5–11) versus BTD(11–12) can be used to identify different regimes of tropical upper tropospheric ice clouds, particularly opaque and nonopaque ice clouds.

3. Trispectral Features at 8.5, 11, and 12 μm From Satellite Measurements

3.1. NASA A-Train Data

[19] The NASA A-Train satellite constellation, currently consisting of five satellites, provides a unique opportunity to detect clouds with close coincidence. The CALIPSO satellite launched on 28 April 2006 combines an active lidar instrument (CALIOP) with passive infrared and visible imagers [*Winker et al.*, 2007]. The CALIOP is a two-wavelength (0.532 and 1.064 μm) lidar that provides high-resolution vertical profiles of thin clouds and aerosols. We note that the CALIOP 0.532 μm channel has polarization capability. Its vertical and horizontal resolutions are 30–60 and 333 m, respectively. The cloud profiling radar (CPR) aboard CloudSat, launched with CALIPSO, is a 94 GHz
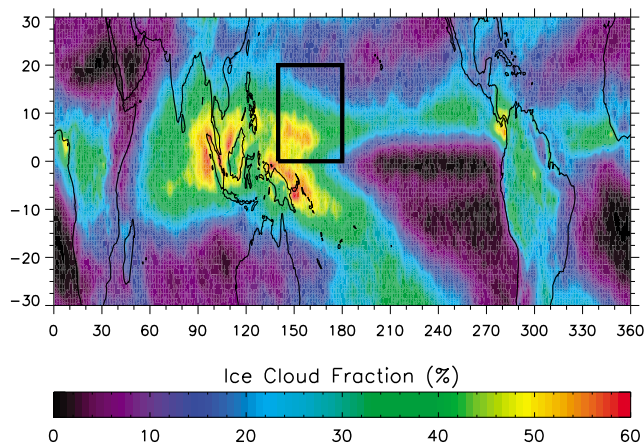
Figure 4. Tropical ice cloud fraction detected by MODIS aboard Aqua satellite in 2007.

nadir-looking radar that measures the power backscattered by clouds as a function of distance from the radar. CPR has the minimum detectable reflectivity of approximately −26 dBZ, a vertical resolution of 500 m, a cross-track resolution of 1.4 km, and an along-track resolution of 1.7 km [*Stephens et al.*, 2002].

[20] MODIS is a key instrument aboard the Aqua (EOS PM) satellite launched on 4 May 2002 as part of the A-Train constellation. A MODIS sensor is also aboard the Terra (EOS AM) satellite. MODIS provides high radiometric sensitivity in 36 spectral bands ranging in wavelengths from 0.4 to 14.4 μm. A ±55° scanning pattern is taken at the EOS orbit of 705 km achieving a swath of 2330 km. Bands 1 and 2 have a nominal resolution of 250 m at nadir, bands 3–7 are 500 m, and bands 8–36 are 1 km. The MODIS visible and near-infrared bands have been used to retrieve daytime cloud optical and microphysical properties [*Platnick et al.*, 2003; *King et al.*, 2004]. Infrared retrieval methods have been used to estimate cloud top temperature and pressure, cloud effective emissivity, and cloud particle phase from measurements taken during both day and night.

[21] The two satellites, CALIPSO and CloudSat, are highly complementary to each other and the combined observations can provide information about the vertical structure of clouds and aerosols unavailable from other Earth observing satellites. The 2B-GEOPROF-LIDAR products [*Mace et al.*, 2007; *Mace and Zhang*, 2008] provide the combined profiles in terms of the spatial grid of the CPR. The cloud top heights from 2B-GEOPROF-LIDAR products are used to identify ice clouds in the upper troposphere.

[22] The level-2 MODIS Collection 5 standard cloud products (MYD06_L2, http://modis.gsfc.nasa.gov/data/dataprod/pdf/MOD_06.pdf) are a narrow-swath MODIS/Aqua subset along the CloudSat field-of-view track. The narrow-swath subset is programmed to select and return MODIS data that are within ±5 km across the CloudSat track. The new subset data are named MODIS/Aqua Clouds 1 and 5 km 5-Min L2 Narrow Swath Subset along CloudSat V2 (MAC06S0, http://mirador.gsfc.nasa.gov/collections/MAC06S0__002.shtml). Depending on the parameters, the MAC06S0 cross-track width is either 3 or 11 pixels. The cloud optical thickness and the effective particle size retrieved from MODIS with 1 km resolution are used in this study. These retrievals use an

algorithm for cloud thermodynamic phase from visible/near-infrared (0.65, 0.86 μm), shortwave-infrared solar reflection (1.64 μm and possibly 2.13 μm), and infrared (8.5 and 11.0 μm) measurements [*King et al.*, 2004]. Since the objective of this study is to use infrared measurements alone, the retrievals of ice cloud optical thickness and effective particle size which are associated with ice phase determined by either BT(8.5) $\leq$ 238 K or BTD(8.5–11) $\geq$ 0.5 K [*Baum et al.*, 2000; *Menzel et al.*, 2006] are used. The standard MODIS Level 1B data set (MYD021_L1, http://modis.gsfc.nasa.gov/data/dataprod/pdf/MOD_02.pdf) contains calibrated and geolocated radiances for all spectral bands. The narrow-swath MODIS/Aqua subset of these data along CloudSat field-of-view track has been subsampled as MODIS/Aqua Calibrated Radiances 1 km 5-min 1B Narrow Swath Subset along CloudSat V2 (MAC021S0, http://mirador.gsfc.nasa.gov/collections/MAC021S0__002.shtml) with a resolution of 1 km. The IR radiances at the 8.5, 11, and 12 μm spectral bands are converted to brightness temperatures to investigate the relationship between BTD (8.5–11) and BTD(11–12) over ice clouds. The MODIS/Aqua Geolocation Fields 1 km 5-min 1A Narrow Swath Subset along CloudSat V2 (MAC03S0, http://mirador.gsfc.nasa.gov/collections/MAC03S0__002.shtml), is the narrow-swath MODIS/Aqua subset along CloudSat field-of-view track, is extracted from geolocation data of 1 km MYD03_L1 (http://modis.gsfc.nasa.gov/data/dataprod/pdf/MOD_03.pdf), and is used to collocate the MAC06S0 and MAC021S0 with 2B-GEOPROF-LIDAR. Since CloudSat, CALIPSO, and MODIS measure the same cloud area within two minutes [*Stephens et al.*, 2002], the nearest-neighbor method within a maximum distance of 0.5 km is used for collocate MODIS and CloudSat/CALIPSO data. Thus, the coincident optical thickness, cloud phase, cloud top height, and IR brightness temperature at 8.5, 11, and 12 μm are available. The present study focused on a region (140°E–180°E, 0°N–20°N) over Western Pacific Warm Pool.

3.2. Properties of IR Radiances at 8.5, 11, and 12 μm of MODIS Over Opaque and Nonopaque Upper Tropospheric Ice Clouds

[23] Figure 4 shows the geographical distribution of tropical ice cloud fractions detected from MODIS during 2007. Ice clouds occur more frequently over the intertropical convergence zone (ITCZ), the South Pacific convergence zone (SPCZ), tropical Africa, the Indian Ocean, and tropical and South America. A region (140°E–180°E, 0°N–20°N) in the Western Pacific Warm Pool with a high frequency of ice clouds is selected to investigate the properties of IR radiances at 8.5, 11, and 12 μm of MODIS. From this region, the collocated optical thickness, cloud phase, cloud top height, and IR brightness temperatures are collected for further analysis.

[24] Figure 5 shows the 2-D histograms of BTD(8.5–11) and BTD(11–12) for opaque ($\tau > 6$) and nonopaque ($\tau < 6$) upper tropospheric ice clouds with the cloud top between 12 and 16 km. The slopes of 2-D histograms of opaque ice clouds are smaller than the slopes of nonopaque ice clouds. Opaque ice clouds also tend to have smaller BTD(8.5–11) than nonopaque ice clouds. It is evident from the values of BTD(8.5–11) and BTD(11–12) that opaque and nonopaque upper tropospheric ice clouds tend to accumulate in different
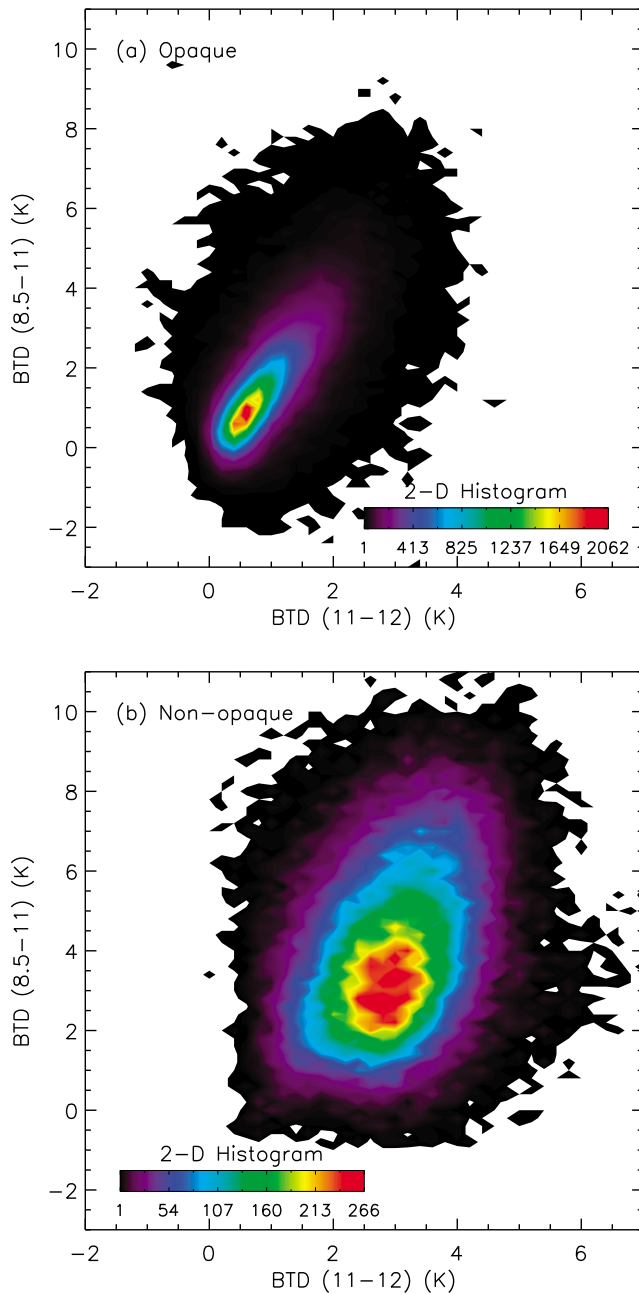
Figure 5. The 2-D histograms of BTD(8.5–11) and BTD (11–12) for (a) opaque and (b) nonopaque upper tropospheric ice clouds.

regions although there are occasional overlapped regions. This feature allows BTD(8.5–11) and BTD(11–12) to be used to identify opaque and nonopaque upper tropospheric ice clouds.

[25] The thresholds suggested for identifying opaque and nonopaque upper tropospheric ice clouds are shown in Figure 6 together with the 2-D histogram of BTD(8.5–11) and BTD(11–12). The thresholds are derived on the basis of statistical training. The lower left of the diagram, separated by the red lines, identifies the opaque upper tropospheric ice clouds, while the remainder of the diagram identifies the nonopaque ice clouds. These criteria successfully identify opaque and nonopaque upper tropospheric ice clouds with

an accuracy of 81.3% (the accuracy is the ratio of the number of correctly identified opaque and nonopaque ice clouds to the total number of ice clouds).

[26] CALIPSO is more sensitive to optically thin cirrus clouds than MODIS. Thus, CALIPSO can profile optically thin cirrus clouds that may be missed by MODIS [*Weisz et al.*, 2007; *Menzel et al.*, 2008]. If multilayer ice clouds occur with an upper-most layer of optically thin cirrus clouds, the lack of detection of the uppermost layer of optically thin cirrus clouds by MODIS may affect IR measurements [*Ham et al.*, 2009; *Davis et al.*, 2009] and induce biases for the detection of opaque and nonopaque tropical upper tropospheric ice clouds from the trispectral technique. If only considering one-layer upper tropospheric ice clouds, the accuracy for opaque and nonopaque ice clouds is improved to be 87.6%.
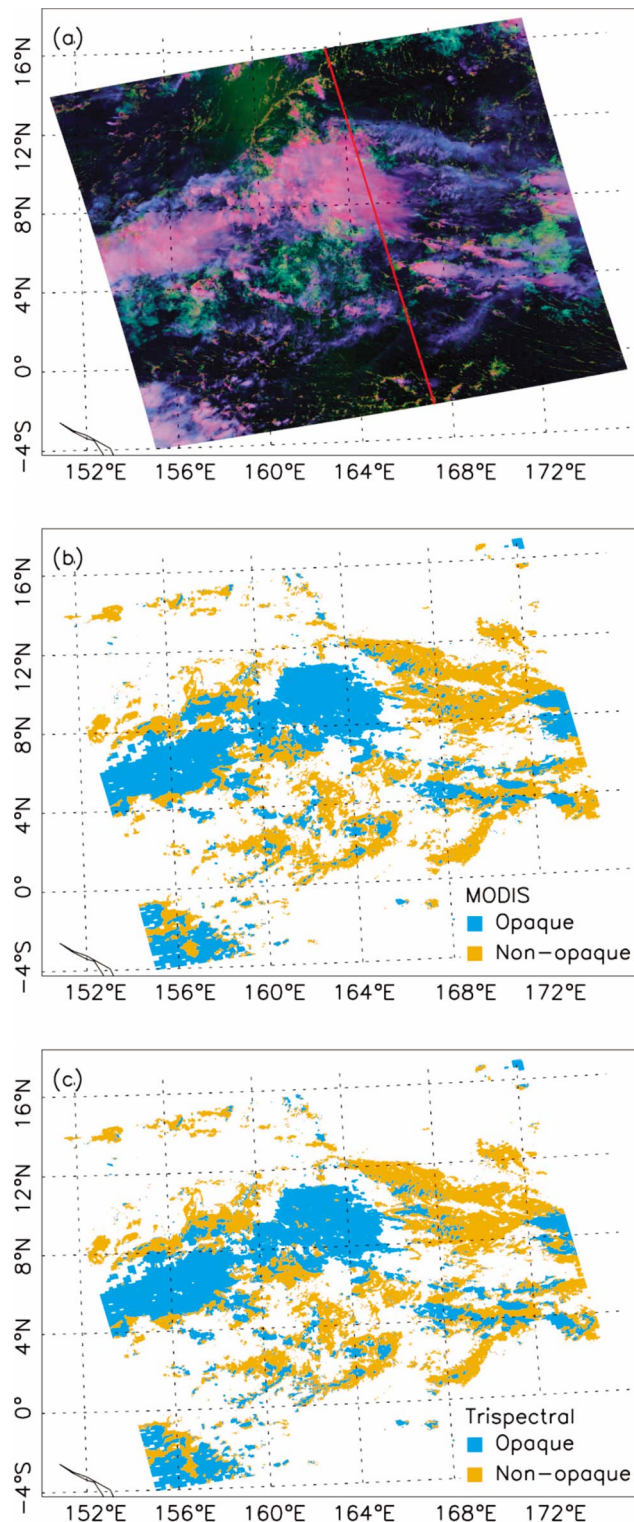
4. Application of Trispectral Features at 8.5, 11, and 12 μm to Identify Opaque and Nonopaque Upper Tropospheric Ice Clouds

[27] The opaque and nonopaque upper tropospheric ice clouds are classified for a MODIS granule over the Western Pacific Warm Pool at 0235 UTC on 27 July 2007. The false color image (Figure 7a) is mapped by the MODIS band 1 reflectance (0.65 μm, red), band 7 reflectance (2.1 μm, green), and band 31 brightness temperature (11 μm, blue) with the scale reversed. Ice clouds appear blue and magenta since ice particle absorption will act to lower the contribution of the 2.11 μm reflectance in the green channel. In order
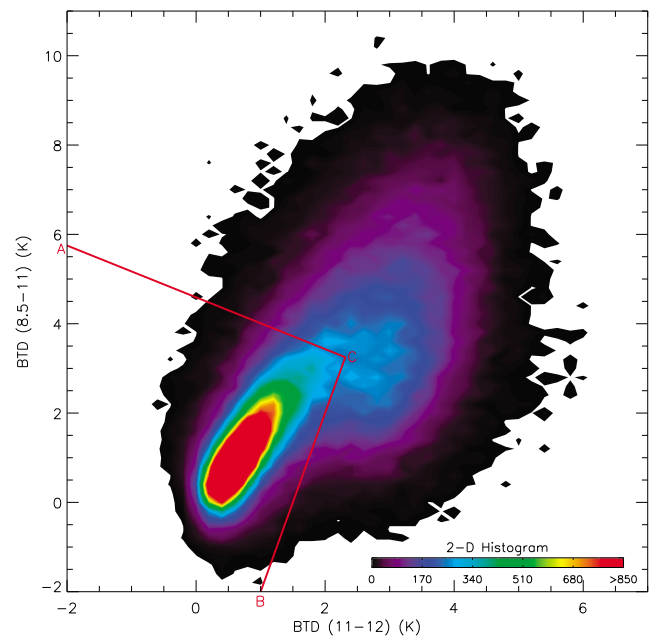
Figure 6. The 2-D histogram of BTD(8.5–11) and BTD (11–12) for upper tropospheric ice clouds. The red lines indicate the criteria for identifying opaque and nonopaque upper tropospheric ice clouds. The region in the lower left is identified as opaque ice clouds and the remaining region is identified as nonopaque ice clouds. The coordinates of points A, B, and C are (−2.0, 5.75), (1.0, −2.0), and (2.31, 3.25), respectively.

Figure 7. (a) The false RGB image based on three Aqua MODIS bands 1, 7, and 31 (gray flipped) (see details in text), observed over the Western Pacific Warm Pool at 0235 UTC on 27 July 2007 (red line indicates the track of CloudSat and CALIPSO crossing this granule), (b) opaque ($\tau > 6$) and nonopaque ($\tau < 6$) upper tropospheric ice clouds from MODIS retrievals, and (c) opaque and nonopaque upper tropospheric ice clouds identified by the present trispectral technique.

to extend the trispectral technique to the entire MODIS granule, the cloud top heights from MODIS retrievals are used to identify the upper tropospheric clouds [*Menzel et al.*, 2008]. Figure 7b shows the opaque ($\tau > 6$) and nonopaque ($\tau < 6$) upper tropospheric ice clouds identified in terms of ice cloud optical thicknesses and cloud top pressures that have been retrieved from MODIS [*Platnick et al.*, 2003; *King et al.*, 2004; *Menzel et al.*, 2008]. The profiles of height and atmospheric pressure from ECMWF along the CloudSat track in the MODIS granule are used to obtain the corresponding cloud top pressures at heights of 12 and 16 km for upper tropospheric ice clouds. The cloud top pressures are about 211 and 108 hPa with standard deviations of about 1.2 and 2.0 hPa. The opaque and nonopaque upper tropospheric ice clouds identified by the trispectral technique (detailed method is shown in Figure 6) are shown in Figure 7c. Evidently, the results from the trispectral technique are consistent with the results directly obtained from MODIS ice cloud retrievals. The accuracy of the classification is 85.1%.

4.1. Effect of Variations in MODIS Zenith Angles

[28] The trispectral technique is applied to MODIS IR measurements along the CloudSat track. These IR measurements are observed at viewing zenith angles that are mostly homogeneous at about 18° with a standard deviation of 0.42°. The effects of variations in MODIS zenith angles on the identifications are investigated by computing the accuracies of identifications over the MODIS granule. The accuracies are 87.9% for $\theta < 15°$, 85.7% for $15° < \theta < 30°$, 82.0% for $30° < \theta < 45°$, and 84.3% for $45° < \theta$. The results indicate that the effects of varying viewing zenith angles on the identified results using the trispectral technique are negligible.

4.2. Effect of the Uncertainties in Cloud Top Pressure

[29] The trispectral technique is developed with help of the CloudSat/CALIPSO derived cloud top heights. To apply this technique to an entire MODIS granule, the cloud top heights from MODIS retrievals are used. In this section, the uncertainties in cloud top heights from MODIS measurements are investigated. *Kokhanovsky et al.* [2009] performed intercomparisons of ground-based radar and satellite cloud top height retrievals for overcast single-layered cloud fields. It was found that the retrievals by MODIS are over 1 km lower than those by radar. *Menzel et al.* [2008] found that the MODIS cloud algorithm produces cloud top pressures that are within 50 hPa (about 1 km) of lidar determinations in single-layer cloud situations. In multi-layer clouds with a semitransparent upper layer cloud, the MODIS-derived cloud top represents the radiative mean between the two cloud layers.

[30] Figure 8 shows ice cloud tops derived from CALIPSO and MODIS along the cross track of CALIPSO in the MODIS granule. Ice cloud vertical structures are shown by CloudSat measurements with a minimum detectable reflectivity of −26 dBZ. It is evident that ice cloud tops from CALIPSO are higher than those derived from MODIS. The latter are closer to the cloud tops identified by CloudSat minimum detectable reflectivity. The effects of the differences in cloud top heights between MODIS and CALISPO on identifying opaque and nonopaque upper tropospheric ice
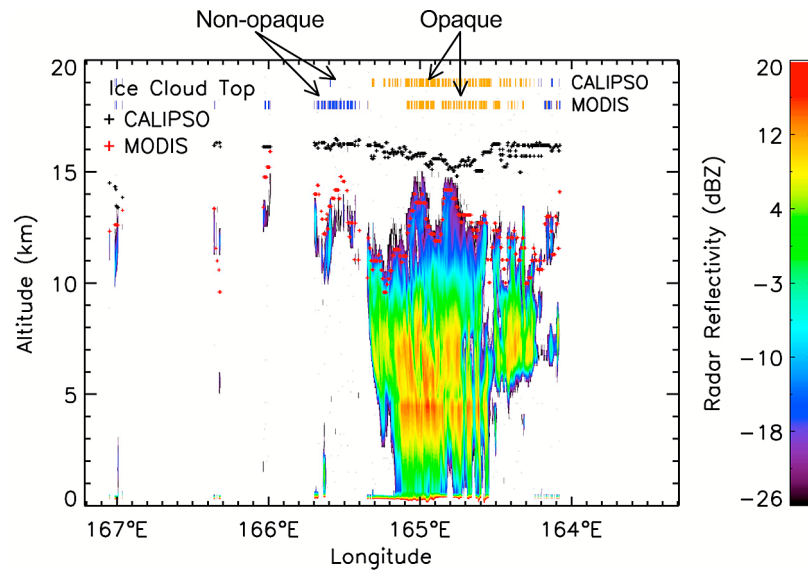
Figure 8. Ice cloud tops derived from CALIPSO and MODIS along the cross track shown in Figure 7a. The orange and blue bars indicate opaque (MODIS retrieved $\tau > 6$) and nonopaque ($\tau < 6$) upper tropospheric ice clouds, respectively, on the basis of cloud tops derived from CALIPSO (top bars) and MODIS (bottom bars). Color contour is for CloudSat radar reflectivity profile.

clouds are shown in Figure 8 by the orange and blue color bars. MODIS retrieved cloud optical thicknesses are used for the identifications.

[31] One year of differences between upper tropospheric ice cloud tops derived from CALIPSO and CloudSat measurements and those from MODIS over the chosen Western Pacific Warm Pool region in 2007 are investigated. It is found that generally ice cloud top heights from CALIPSO are higher than those from MODIS because CALIPSO is more sensitive to the presence of ice particles at cloud top, while a passive radiometer such as MODIS responds to the radiometric signature of a cloud having an optical thickness of about 1 [*Holz et al.*, 2008]. In other words, the MODIS approach tends to place a cloud at a height below the presence of the first ice particles. For an optically thick cloud, the MODIS and CALIPSO will correspond well, while for the case of a geometrically thick, but optically thin, ice cloud, there will be greater differences in perceived heights. The mean and standard deviation values of these differences are 2.3 and 1.8 km, respectively. Considering upper tropospheric ice clouds with a MODIS cloud top within 4 km of CALIPSO determinations, the present trispectral technique identified nonopaque and opaque ice clouds with an accuracy of 87.7%.

5. Conclusions

[32] In this study, a trispectral technique is suggested to discriminate between tropical upper tropospheric opaque ($\tau > 6$) and nonopaque ($\tau < 6$) ice clouds over ocean from analysis of the brightness temperature differences between 8.5 and 11 μm bands [BTD(8.5–11)] and those between 11 and 12 μm bands [BTD(11–12)] from MODIS together with MODIS detected cloud thermodynamic phase. The detection can be used as a precursor to an infrared optical thickness

retrieval, which is not available for the current MODIS ice cloud product.

[33] The integrated measurements from the MODIS airborne simulator (MAS), cloud physics lidar (CPL), and cloud radar system (CRS) aboard the NASA ER-2 aircraft during the CRYSTAL-FACE experiment in 2002 are used to investigate the trispectral features of BTD(8.5–11) and BTD(11–12) of ice clouds. The simultaneous measurements along three tracks over tropical ice anvil systems on 29 July 2002 are investigated. It is found that the combination of BTD(8.5–11) and BTD(11–12) can be used to classify ice clouds.

[34] One year of collocated measurements from MODIS, CALIPSO, and CloudSat in the A-Train constellation, taken over a region (140°E–180°E, 0°N–20°N) in the Western Tropical Warm Pool, are analyzed to investigate the performance of our approach. MODIS retrieved ice cloud optical thicknesses and CALIPSO and CloudSat derived cloud top heights are used to identify upper tropospheric opaque and nonopaque ice clouds. These identified opaque and nonopaque ice clouds are used to investigate the trispectral features of corresponding MODIS measured BTD (8.5–11) and BTD(11–12). Furthermore, the pronounced trispectral features are used to identify opaque and nonopaque upper tropospheric ice clouds. The accuracy of identifying opaque and nonopaque upper tropospheric ice clouds using the trispectral technique is 81.3%. If only considering single-layered ice clouds, the accuracy of these detections is improved by 6.3%. This is due to the decrease in the influence of multiple layers of ice clouds, particularly those with an upper layer of optically thin cirrus cloud undetected by MODIS but identified by CALIPSO.

[35] With the application of the trispectral technique to MODIS, opaque and nonopaque upper tropospheric ice clouds are classified for a MODIS granule over the Western Pacific Warm Pool on 27 July 2007 by combing the cloud

top heights from MODIS retrievals. The classifications from the trispectral technique are consistent with those directly classified from the MODIS ice cloud optical thicknesses. The effect of the variations in MODIS zenith angles on the trispectral technique is investigated by grouping the identifications over the granule on the basis of the different zenith angles. It is found that the variations in MODIS zenith angles have negligible effects on the identified results. In the variation range of cloud top differences of 2.3 ± 1.8 km (values of mean and standard deviation), the accuracy for detecting opaque and nonopaque upper tropospheric ice clouds is 85.1%.

References

Ackerman, S. A., W. L. Smith, and H. E. Revercomb (1990), The 27–28 October 1986 FIRE IFO cirrus case study: Spectral properties of cirrus clouds in the 8–12 μm window, *Mon. Weather Rev.*, 118, 2377–2388.

Baum, B. A., P. F. Soulen, K. I. Strabala, M. D. King, S. A. Ackerman, W. P. Menzel, and P. Yang (2000), Remote sensing of cloud properties using MODIS airborne simulator imagery during SUCCESS: II. Cloud thermodynamic phase, *J. Geophys. Res.*, 105, 11,781–11,792, doi:10.1029/1999JD901090.

Baum, B. A., R. A. Frey, G. G. Mace, M. K. Harkey, and P. Yang (2003), Nighttime multilayered cloud detection using MODIS and ARM data, *J. Appl. Meteorol.*, 42(7), 905–919.

Chen, T., W. B. Rossow, and Y.-C. Zhang (2000), Radiative effects of cloud-type variations, *J. Climate*, 13, 264–286.

Comstock, J. M., et al. (2007), An intercomparison of microphysical retrieval algorithms for upper tropospheric ice clouds, *Bull. Am. Meteorol. Soc.*, 88, 191–204.

Corti, T., B. P. Luo, Q. Fu, H. Vomel, and T. Peter (2006), The impact of cirrus clouds on tropical troposphere to stratosphere transport, *Atmos. Chem. Phys.*, 6, 2539–2547.

Davis, S. M., L. M. Avallone, B. H. Kahn, K. G. Meyer, and D. Baumgardner (2009), Comparison of airborne in situ measurements and moderate resolution imaging spectroradiometer (MODIS) retrievals of cirrus cloud optical and microphysical properties during the midlatitude cirrus experiment (MidCiX), *J. Geophys. Res.*, 114, D02203, doi:10.1029/2008JD010284.

Dessler, A. E., S. P. Palm, W. D. Hart, and J. D. Spinhirne (2006), Tropopause-level thin cirrus coverage revealed by ICESat/geoscience laser altimeter system, *J. Geophys. Res.*, 111, D08203, doi:10.1029/2005JD006586.

Eguchi, N., T. Yokota, and G. Inoue (2007), Characteristics of cirrus clouds from ICESat/GLAS observations, *Geophys. Res. Lett.*, 34, L09810, doi:10.1029/2007GL029529.

Fu, Q., Y. Hu, and Q. Yang (2007), Identifying the top of the tropical tropopause layer from vertical mass flux analysis and CALIPSO lidar cloud observations, *Geophys. Res. Lett.*, 34, L14813, doi:10.1029/2007GL030099.

Gao, R.-S., et al. (2004), Evidence that nitric acid increases relative humidity in cirrus clouds, *Science*, 303, 516–520.

Gettelman, A., and T. Birner (2007), Insights into tropical tropopause layer processes using global models, *J. Geophys. Res.*, 112, D23104, doi:10.1029/2007JD008945.

Gettelman, A., M. L. Salby, and F. Sassi (2002), The distribution and influence of convection in the tropical tropopause region, *J. Geophys. Res.*, 107(D10), 4080, doi:10.1029/2001JD001048.

Ham, S.-H., B.-J. Sohn, P. Yang, and B. A. Baum (2009), Assessment of the quality of MODIS cloud products from radiance simulations, *J. Appl. Meteorol. Climatol.*, 48, 1591–1611.

Hartmann, D. L., J. R. Holton, and Q. Fu (2001), The heat balance of the tropical tropopause, cirrus, and stratospheric dehydration, *Geophys. Res. Lett.*, 28, 1969–1972, doi:10.1029/2000GL012833.

Heidinger, A. K., and M. J. Pavolonis (2009), Gazing at cirrus clouds for 25 years through a split window: Part 1. Methodology, *J. Appl. Meteorol. Climatol.*, 48, 110–1116.

Holz, R. E., S. A. Ackerman, F. W. Nagle, R. Frey, S. Dutcher, R. E. Kuehn, M. Vaughan, and B. A. Baum (2008), Global MODIS cloud detection and height evaluation using CALIOP, *J. Geophys. Res.*, 113, D00A19, doi:10.1029/2008JD009837.

Hook, S. J., J. J. Myers, K. J. Thome, M. Fitzgerald, and A. B. Kahle (2001), The MODIS/ASTER airborne simulator (MASTER) – A new instrument for Earth science studies, *Remote Sens. Environ.*, 76, 93–102.

Hong, G., G. Heygster, J. Miao, and K. Kunzi (2005), Detection of tropical deep convective clouds from AMSU-B water vapor channels measurements, *J. Geophys. Res.*, 110, D05205, doi:10.1029/2004JD004949.

Hong, G., P. Yang, H.-L. Huang, B. A. Baum, Y.-X. Hu, and S. Platnick (2007a), The sensitivity of ice cloud optical and microphysical passive satellite retrievals to cloud geometrical thickness, *IEEE Trans. Geosci. Remote Sens.*, 45, 1315–1323.

Hong, G., P. Yang, B.-C. Gao, B. A. Baum, Y. X. Hu, M. D. King, and S. Platnick (2007b), High cloud properties from three years of MODIS Terra and Aqua data over the tropics, *J. Appl. Meteorol. Climatol.*, 46, 1840–1856.

Hong, G., P. Yang, F. Weng, and Q. Liu (2008), Microwave scattering properties of sand particles: Application to the simulation of microwave radiances over sandstorms, *JQSRT*, 109, 684–702.

Huang, X., and H. Su (2008), Cloud radiative effect on tropical troposphere to stratosphere transport represented in a large-scale model, *Geophys. Res. Lett.*, 35, L21806, doi:10.1029/2008GL035673.

Immler, F., K. Krüger, S. Tegtmeier, M. Fujiwara, P. Fortuin, G. Verver, and O. Schrems (2007), Cirrus clouds, humidity, and dehydration in the tropical tropopause layer observed at Paramaribo, Surinam (5.8°N, 55.2°W), *J. Geophys. Res.*, 112, D03209, doi:10.1029/2006JD007440.

Inoue, T. (1987), A cloud type classification with NOAA7 split-window measurements, *J. Geophys. Res.*, 92, 3991–4000, doi:10.1029/JD092iD04p03991.

Inoue, T. (1989), Features of clouds over the tropical Pacific during northern hemispheric winter derived from split window measurements, *J. Meteorol. Soc. Jpn.*, 67, 621–637.

Jensen, E., and L. Pfister (2004), Transport and freeze-drying in the tropical tropopause layer, *J. Geophys. Res.*, 109, D02207, doi:10.1029/2003JD004022.

Kahn, B. H., K. N. Liou, S.-Y. Lee, E. F. Fishbein, S. DeSouza-Machado, A. Eldering, E. J. Fetzer, S. E. Hannon, and L. L. Strow (2005), Nighttime cirrus detection using atmospheric infrared sounder window channels and total column water vapor, *J. Geophys. Res.*, 110, D07203, doi:10.1029/2004JD005430.

King, M. D., et al. (1996), Airborne scanning spectrometer for remote sensing of cloud, aerosol, water vapor, and surface properties, *J. Atmos. Ocean. Tech.*, 13, 777–794.

King, M. D., S. Platnick, P. Yang, G. T. Arnold, M. A. Gray, J. C. Riédi, S. A. Ackerman, and K.-N. Liou (2004), Remote sensing of liquid water and ice cloud optical thickness and effective radius in the Arctic: Application of airborne multispectral MAS data, *J. Atmos. Ocean. Tech.*, 21, 857–875.

Kokhanovsky, A. A., C. M. Naud, and A. Devasthale (2009), Intercomparison of ground-based satellite cloud top height retrievals for overcast single-layered cloud fields, *IEEE Trans. Geosci. Remote Sens.*, 47, 1901–1908.

Li, L., G. M. Heymsfield, P. E. Racette, L. Tian, and E. Zenker (2004), A 94 GHz cloud radar system on a NASA high-altitude ER-2 aircraft, *J. Atmos. Ocean. Tech.*, 21, 1378–1388.

Luo, B. P., et al. (2003), Dehydration potential of ultrathin clouds at the tropical tropopause, *Geophys. Res. Lett.*, 30(11), 1557, doi:10.1029/2002GL016737.

Lutz, H. J., T. Inoue, and J. Schmetz (2003), Comparison of a splitwindow and a multispectral cloud classification for MODIS observations, *J. Meteorol. Soc. Jpn.*, 81(3), 623–631.

Mace, G. G., R. Marchand, and G. L. Stephens (2007), Global hydrometeor occurrence as observed by CloudSat; Initial observations from summer 2006, *Geophys. Res. Lett.*, 34, L09808, doi:10.1029/2006GL029017.

Mace, G., and Q. Zhang (2008), 2B-GEOPROF-LIDAR Interface Control Document, 2B-GEOPROF-LIDAR Product Version: 003 (26 November 2008), CloudSat Project, A NASA Earth System Science Pathfinder Mission.

McFarquhar, G., A. Heymsfield, J. Spinhirne, and B. Hart (2000), Thin and subvisual tropopause tropical cirrus: Observations and radiative impact, *J. Atmos. Sci.*, 57, 1841–1853.

McGill, M. J., D. L. Hlavka, W. D. Hart, J. D. Spinhirne, V. S. Scott, and B. Schmid (2002), The cloud physics lidar: Instrument description and initial measurement results, *Appl. Opt.*, *41*(18), 3725–3734.

McGill, M. J., L. Li, W. D. Hart, G. M. Heymsfield, D. L. Hlavka, P. E. Racette, L. Tian, M. A. Vaughan, and D. M. Winker (2004), Combined lidar-radar remote sensing: Initial results from CRYSTAL-FACE, *J. Geophys. Res.*, *109*, D07203, doi:10.1029/2003JD004030.

Menzel, W. P., R. A. Frey, H. Zhang, D. P. Wylie, C. C. Moeller, R. A. Holz, B. Maddux, B. A. Baum, K. I. Strabala, and L. E. Gumley (2008), MODIS global cloud top pressure and amount estimation: Algorithm description and results, *J. Appl. Meteorol. Climatol.*, *47*, 1175–1198.

Menzel, W. P., R. A. Frey, B. A. Baum, and H. Zhang (2006), MODIS cloud top properties and cloud phase algorithm theoretical basis document, http://modis.gsfc.nasa.gov/data/atbd/atbd_mod04.pdf.

Minnis, P., et al. (1995), Cloud Optical Property Retrieval (Subsystem 4.3), in *Clouds and the Earth's Radiant Energy System (CERES) Algorithm Theoretical Basis Document, Volume III: Cloud Analyses and Radiance Inversions (Subsystem 4)*, *NASA RP 1376 Vol 3*, edited by CERES Science Team, pp. 135–176.

Minnis, P., D. P. Garber, D. F. Young, R. F. Arduini, and Y. Takano (1998), Parameterizations of reflectance and effective emittance for satellite remote sensing of cloud properties, *J. Atmos. Sci.*, *55*, 3313–3339.

Nasiri, S. L., and B. H. Kahn (2008), Limitations of bi-spectral infrared cloud phase determination and potential for improvement, *J. Appl. Meteorol. Climatol.*, *47*, 2895–2910.

Pavolonis, M. J., A. K. Heidinger, and T. Uttal (2005), Daytime global cloud typing from AVHRR and VIIRS: Algorithm description, validation, and comparisons, *J. Appl. Meteorol.*, *44*, 804–826.

Platnick, S., M. D. King, S. A. Ackerman, W. P. Menzel, B. A. Baum, J. C. Riédi, and R. A. Frey (2003), The MODIS cloud products: Algorithms and examples from Terra, *IEEE Trans. Geosci. Remote Sens.*, *41*(2), 459–473.

Poetzsch-Heffter, C., Q. Liu, E. Ruprecht, and C. Simmer (1995), Effect of cloud types on the Earth Radiation Budget calculated with the ISCCP C1 data set: Methodology and initial results, *J. Climate*, *8*, 829–843.

Racette, P. E., G. M. Heymsfield, L. Li, L. Tian, and E. Zenker (2003), The cloud radar system, 31st Conf. on Radar Meteorology, Seattle, WA, *Am. Meteorol. Soc.*, 237–240.

Ramanathan, V., and W. Collins (1991), Thermodynamic regulation of ocean warming by cirrus clouds deduced from observations of the 1987 El Niño, *Nature*, *351*, 27–32.

Rossow, W. B., and R. A. Schiffer (1999), Advances in understanding clouds from ISCCP, *Bull. Am. Meteorol. Soc.*, *80*, 2261–2288.

Rossow, W. B., and Y.-C. Zhang (1995), Calculation of surface and top of atmosphere radiative fluxes from physical quantities based on ISCCP data sets: 2. Validation and first results, *J. Geophys. Res.*, *100*, 1167–1197, doi:10.1029/94JD02746.

Stephens, G. L. (2005), Cloud feedbacks in the climate system: A critical review, *J. Climate*, *18*, 237–273.

Stephens, G. L., et al. (2002), The CloudSat mission and the A-TRAIN: A new dimension to space-based observations of clouds and precipitation, *Bull. Am. Meteorol. Soc.*, *83*, 1771–1790.

Strabala, K. I., S. A. Ackerman, and W. P. Menzel (1994), Cloud properties inferred from 8–12 μm data, *J. Appl. Meteorol.*, *33*, 212–229.

Stubenrauch, C. J., A. Chédin, G. Rädel, N. A. Scott, and S. Serrar (2006), Cloud properties and their seasonal and diurnal variability from TOVS Path-B, *J. Climate*, *19*, 5531–5553.

Tian, B., I. M. Held, N.-C. Lau, and B. J. Soden (2005), Diurnal cycle of summertime deep convection over North America: A satellite perspective, *J. Geophys. Res.*, *110*, D08108, doi:10.1029/2004JD005275.

Wang, P. H., P. Minnis, M. P. McCormick, G. S. Kent, and K. M. Skeens (1996), A 6-year climatology of cloud occurrence frequency from stratospheric aerosol and gas experiment II observations (1985–1990), *J. Geophys. Res.*, *101*, 29,407–29,429, doi:10.1029/96JD01780.

Weisz, E., J. Li, W. P. Menzel, A. K. Heidinger, B. H. Kahn, and C.-Y. Liu (2007), Comparison of AIRS, MODIS, CloudSat and CALIPSO cloud top height retrievals, *Geophys. Res. Lett.*, *34*, L17811, doi:10.1029/2007GL030676.

Winker, D. M., W. H. Hunt, and M. J. McGill (2007), Initial performance assessment of CALIOP, *Geophys. Res. Lett.*, *34*, L19803, doi:10.1029/2007GL030135.

Wylie, D. P., D. L. Jackson, W. P. Menzel, and J. J. Bates (2005), Trends in global cloud cover in two decades of HIRS observations, *J. Climate*, *18*, 3021–3031.

Wylie, D. P., and W. P. Menzel (1999), Eight years of high cloud statistics using HIRS, *J. Climate*, *12*, 170–184.

Zhang, Y.-C., W. B. Rossow, and A. A. Lacis (1995), Calculation of surface and top-of-atmosphere radiative fluxes from physical quantities based on ISCCP data sets: 1. Method and sensitivity to input data uncertainties, *J. Geophys. Res.*, *100*, 1149–1165, doi:10.1029/94JD02747.

B. A. Baum, Space Science and Engineering Center, University of Wisconsin Madison, Madison, WI 53706, USA.

A. K. Heidinger and M. J. Pavolonis, NOAA/NESDIS Center for Satellite Applications and Research, Madison, WI, USA.

G. Hong and P. Yang, Department of Atmospheric Sciences, Texas A&M University, College Station, TX 77843, USA. (hong@ariel.met.tamu.edu)

S. E. Platnick, Laboratory for Atmospheres, NASA-GSFC, Greenbelt, MD, USA.